nature structural & molecular biology

Conformational ensemble of the sodium-coupled aspartate transporter

Elka R Georgieva[1,2], Peter P Borbat[1,2], Christopher Ginter[3], Jack H Freed[1,2] & Olga Boudker[3]

Sodium and aspartate symporter from *Pyrococcus horikoshii*, Glt_{Ph}, is a homolog of the mammalian glutamate transporters, homotrimeric integral membrane proteins that control neurotransmitter levels in brain synapses. These transporters function by alternating between outward-facing and inward-facing states, in which the substrate binding site is oriented toward the extracellular space and the cytoplasm, respectively. Here we used double electron-electron resonance (DEER) spectroscopy to probe the structure and the state distribution of the subunits in the trimer in distinct hydrophobic environments of detergent micelles and lipid bilayers. Our experiments reveal a conformational ensemble of protomers that sample the outward-facing and inward-facing states with nearly equal probabilities, indicative of comparable energies, and independently of each other. On average, the distributions varied only modestly in detergent and in bilayers, but in several mutants unique conformations were stabilized by the latter.

Glutamate is a major excitatory neurotransmitter in the central nervous system and is crucial in learning, memory formation and cognition[1]. Although glutamate is abundant in the brain, its extracellular concentration is tightly controlled to allow for neurotransmission; abnormally elevated levels of glutamate observed in several neurodegenerative diseases, ischemia and epilepsy are toxic[2]. Glutamate transporters are electrochemically driven pumps, which couple uptake of glutamate into the cytoplasm of astrocytes and neurons to the thermodynamically 'downhill' movements of ions[3–5]. The structural information for this family comes from the crystal structures of an archaeal homolog, Glt_{Ph}[6–9], a sodium and aspartate symporter[7,10,11], which has ~35% amino acid sequence identity with the mammalian glutamate transporters and is a model system to study their mechanism. The crystal structures revealed a homotrimeric assembly, common for all characterized members of the family[12,13]. Each protomer has an independent set of aspartate and sodium (Na^+) binding sites at the core of a peripherally located transport domain (**Fig. 1a**). The central transmembrane segments form the trimerization domain, mediating intersubunit contacts and remaining largely unchanged during transport[8,9,14]. In contrast, transport domains exhibit structural plasticity, leading to 15–18 Å movements across the membrane, thereby switching the substrate and ion-binding sites between the extracellular and cytoplasmic orientations, that is, the outward-facing and inward-facing states, respectively. Two reentrant hairpin segments of the transport domain, hairpins 1 and 2 (HP1 and HP2), occlude the substrate and ions from the aqueous milieus in both states, and HP2 has been proposed to serve as an extracellular gate[7,15–17]. Aspartate binding and closure of the extracellular gate are thermodynamically coupled to binding of Na^+ ions[7]. In contrast, isomerization between the outward-facing and inward-facing states has been proposed to occur independently of the ions, driven primarily by the thermal energy[8].

Here we aimed to gain structural information on outward-facing and inward-facing states of Glt_{Ph} and to establish their energetic relationship in two distinct hydrophobic environments, namely in detergent micelles and in lipid bilayers. In this way we begin to sketch out the energy profile of the transport cycle. Toward this end, we used site-directed spin labeling and DEER spectroscopy to measure the distances between the paramagnetic probes. The technique provides access to distances and, notably, distance distributions ranging from 20 Å to over 80 Å[18–21], and has been applied to study diverse systems, including membrane proteins in lipid bilayers[20,22–29]. Here we broaden the applicability of DEER spectroscopy by extracting quantitative information on the populations and the energies of the conformational states contributing to the experimentally observed distance distributions.

We used spin-labeled cysteine mutants of Glt_{Ph} for the long-range distance measurements either when the transporters were empty or loaded with Na^+ ions and aspartate or a transport blocker DL-*threo*-β-benzoxyaspartate (TBOA). We obtained broad distance distributions, which we interpret in terms of an ensemble of the underlying inward-facing and outward-facing states, consistent with the known crystal structures. The quantitative analysis revealed that the two states were populated with almost equal probabilities under all conditions, indicating similar energies. Moreover, our data are consistent with a lack of cooperativity in the trimers, painting a picture of a system in which each protomer samples outward-facing and inward-facing conformations independently of its neighbors, regardless of whether it is loaded with the substrate or is empty. On average, we found no

[1]National Biomedical Center for Advanced Electron Spin Resonance Technology, Cornell University, Ithaca, New York, USA. [2]Department of Chemistry and Chemical Biology, Cornell University, Ithaca, New York, USA. [3]Weill Cornell Medical College, Department of Physiology and Biophysics, New York, New York, USA. Correspondence should be addressed to O.B. (olb2003@med.cornell.edu).

Received 14 June 2012; accepted 17 December 2012; published online 20 January 2013; doi:10.1038/nsmb.2494

substantial differences in either the structure or the relative energies of the outward-facing and inward-facing states in detergent micelles and in lipid bilayers. However, in several mutants, in which the spin label was placed on the interface between the transport and trimerization domains in one of the states, we saw substantial stabilization of those states in lipid but not in detergent. These results suggest that the spin label participates in specific protein interactions and that these interactions are more favorable when the transporter is embedded into membrane compared to detergent micelles.

RESULTS

Spin-labeling strategy

Isomerization of Glt_{Ph} between the outward-facing and inward-facing states as seen by crystallography[6–8] involves ~15 Å translation and 35° rotation of the transport domains relative to the trimerization domain (**Fig. 1a**). As a result, the intersubunit distances between equivalent residues in the transport domains change by up to 20 Å, providing a means to distinguish the states. For single-cysteine mutagenesis and labeling, we selected residues that are solvent-accessible in at least one of the conformations and for which the intersubunit distances are ~20–70 Å, which are most suitable for DEER analysis (**Fig. 1b**, and **Supplementary Table 1**). Specifically, we chose two regions distant from the substrate-binding and ion-binding sites, one on each the cytoplasmic and the extracellular side, and the third region on HP2 (**Fig. 1c**). Two residues in the trimerization domain, which is expected to remain rigid upon substrate binding or translocation, served as controls. We spin-labeled the purified cysteine mutants and conducted DEER measurements (**Supplementary Fig. 1** and **Supplementary Note**) either in detergent (*n*-dodecyl-β-D-maltopyranoside; DDM) or after reconstitution into lipid bilayers (1-palmitoyl-2-oleoylphosphatidylcholine; POPC).

Structural stability of the trimerization domain

For the labeled trimerization domain mutant, K55R1 (R1 denotes a spin-labeled cysteine), the amplitude of the DEER signal at zero time in detergent was consistent with complete spin labeling of cysteines (**Fig. 2a**, **Supplementary Fig. 2a** and **Supplementary Note**). The clear oscillations in the time evolution signal indicated a narrow range of the interspin distances. The extracted distance distributions covered a range between 18 Å and 30 Å for the substrate-free apo Glt_{Ph} and the transporter bound to Na^+ and aspartate or to TBOA. We obtained similar results in detergent and lipid. The distribution medians (**Fig.2b**) varied between 23 Å and 28 Å, in excellent agreement with the C_β-C_β interprotomer distances in the crystal structures of the outward-facing and inward-facing Glt_{Ph} (**Fig. 1b** and **Supplementary Table 1**). The distribution widths (2.8–4.6 Å) were similar to those obtained for soluble well-folded proteins[30–32] and likely originated mainly from the conformational flexibility of the R1 side chain.

We obtained similar but distinct signals for Glt_{Ph}-K55R in the apo state and when bound to either aspartate or TBOA, particularly in detergent. Residue 55 is at the interface of the transport and trimerization domains, and likely experiences distinct steric constraints in the outward-facing and inward-facing states, which may underlie differences in the interspin distances. To test this, we computed theoretical distance distributions based on energy-weighted R1 rotamer libraries generated by a modeling program MMM[33] using crystallographic structures of Glt_{Ph} in the symmetric outward-facing and inward-facing states along with a model of an asymmetric trimer with two protomers in the outward-facing state and one in the inward-facing state (Online Methods). Modeling suggested that R1 in position 55 was more sterically constrained in the inward-facing conformation with fewer accessible rotamers (**Fig. 2c** and **Supplementary Fig. 2b**). Notably, experimental distance distributions encompassed predicted features of both the outward-facing and inward-facing states, suggesting that both were populated. We obtained similar results for V216R1 mutant, located in a more flexible peripheral part of the trimerization domain. Consistently, the experimental distance distributions were broader with widths of 5.2–7.6 Å (**Supplementary Fig. 3** and **Supplementary Table 1**).

To evaluate potential contributions from the three-spin effects to the apparent distance distributions[34,35], we collected DEER data

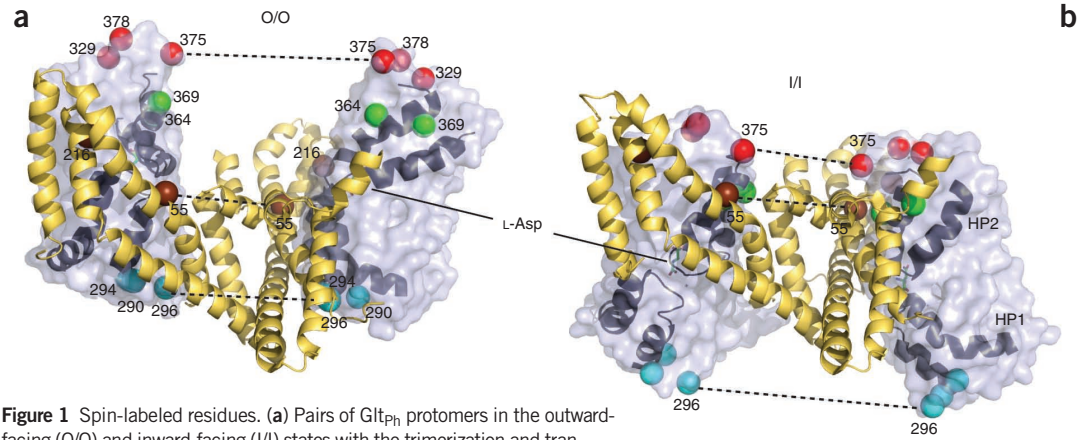

Residue	O/O	I/I
55	28	28
216	54	54
290	38	59
294	45	59
296	32	49
329	65	46
364	44	32
369	57	34
375	44	26
378	57	42

Figure 1 Spin-labeled residues. (**a**) Pairs of Glt_{Ph} protomers in the outward-facing (O/O) and inward-facing (I/I) states with the trimerization and transport domains shown in cartoon (yellow) and transparent surface (blue) representations, respectively. For clarity, the third protomer was removed. The C_β atoms of the residues mutated to cysteines are shown as spheres and colored by region: trimerization domain, brown; intracellular side of the transport domain, blue; extracellular side of the transport domain, red; and HP2, green. (**b**) C_β-C_β distances for mutated residues in symmetrical protomer pairs in outward-facing (O/O) and inward-facing (I/I) states. (**c**) Topology of a Glt_{Ph} protomer with spin-labeled residues shown as spheres with residue number given and colored as in **a**. Numbers at the bottom indicate the transmembrane segments.

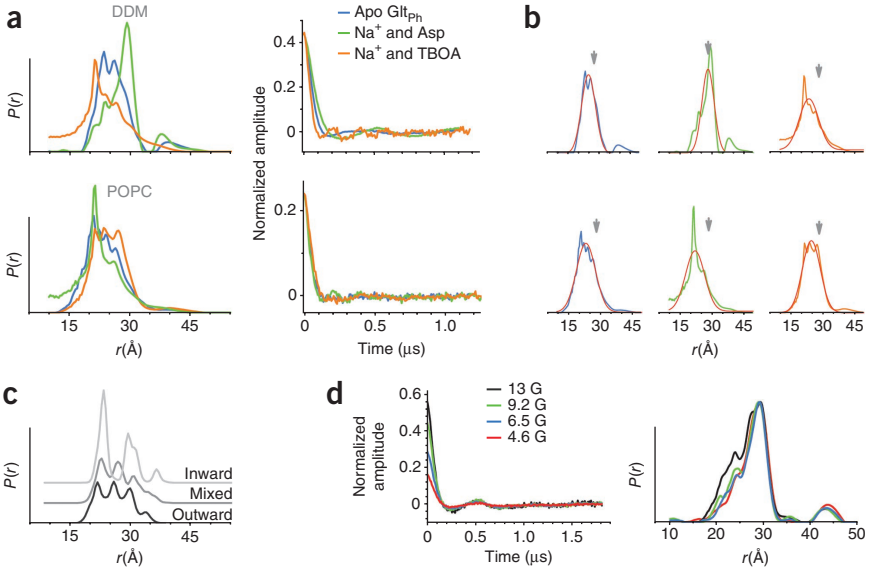

Figure 2 Narrow distance distributions of trimerization domain residue 55. (**a**) Distance distributions (left) and time-domain data (right) for K55R1 in detergent (DDM) and in lipid (POPC). Distance distributions were normalized to the integral of unity; *r* indicates distance; *P*(*r*) indicates the distance probability. Data are for the apo Glt_{Ph}, and for the transporter bound to Na^+ and aspartate (Asp) or Na^+ and TBOA. (**b**) Experimental distances for transporter states indicated and colored as in **a**, and single Gaussian approximations (red) for detergent (top) and lipid (bottom). Arrows at 28 Å correspond to C_β-C_β distance in the crystal structures. (**c**) Distance distributions predicted from the rotamer libraries. Distance probabilities are distributed vertically for clarity. (**d**) Time-domain data and distance distributions obtained using pump pulse of 13 (black), 9.2 (green), 6.5 (blue) and 4.6 G (red).

on Glt_{Ph}-K55R1 using pump pulses with decreasing amplitude (**Supplementary Note**). As expected for a three-spin system, strong pulses of 13 gauss (G) yielded an extra peak around ~23 Å, which was diminished when we used weaker pulses that flipped only a fraction of the spins (**Fig. 2d**). Therefore, in subsequent experiments we used a 5.6-G pump pulse, which rendered the three-spin effects negligible.

Dynamic nature of the transport domain

We collected DEER data on eight transport domain mutants in detergent and lipid membranes either in the apo state or bound to Na^+ and aspartate or to TBOA, yielding 44 different samples. We obtained very broad distance distributions, spanning up to 40–50 Å, for almost all samples except in a few cases (**Fig. 3** and **Supplementary Fig. 4**). In most of the detergent-containing samples, additions of Na^+ and aspartate or Na^+ and TBOA shifted the distance-distribution midpoints toward longer distances in the extracellular mutants (by an average of 2.2 Å or 4.3 Å, respectively) and toward shorter distances in the intracellular mutants (by ~2.8 Å or 3 Å, respectively). These systematic changes suggest that the broad distance distributions are not due to local flexibility but arise from Glt_{Ph} protomers populating independently both the outward-facing and inward-facing states, and that binding of both aspartate and TBOA in detergent favors the outward-facing state to some extent. It is, in principle, possible that the distance distributions are due to the protomers sampling not only the fully outward-facing and inward-facing states but the intermediate positions as well. Indeed, a recent crystal structure has captured a Glt_{Ph} protomer in an intermediate orientation[9], suggesting that the energies of the intermediate states may not be prohibitively high. However, we think that the intermediates do not contribute to the conformational ensemble because the distributions obtained in the presence of TBOA are similarly broad. The benzyl group of TBOA is expected to prevent the occlusion of the inhibitor in the binding site, disabling translocation[7,36]. Therefore, the broad distributions must originate from the contributions of Glt_{Ph} protomer pairs in discrete configurations. Modeling also showed that the experimental distance distributions could not be explained by a single conformation because they covered the distances predicted for both states (**Supplementary Fig. 4**). These observations suggest that in detergent solutions and in lipid bilayers, both in the bound and unbound states, Glt_{Ph} protomers are distributed between the outward-facing and inward-facing conformations.

Conformational selection in the lipid bilayer

Overall, distance distributions were similarly broad in detergent micelles and in lipid bilayers. However, there were several exceptions, including K290R1 bound to TBOA, E296R1 in either apo or bound states and A364R1 bound to aspartate, for which the distributions were broad in detergent but narrow in the bilayers. Particularly for residue 296, we observed very narrow peaks in the distance distributions, indicative of steric constraints on R1 mobility. The distribution medians in the bilayers were consistent with the outward orientation of the intracellular mutants K290R1 and E296R1, and inward orientation of the extracellular mutant A364R1. The crystal structures suggest that these residues are not in a direct contact with the lipid in either the outward-facing or inward-facing states. If this is the case, why do the R1 side chains stabilize specific states in lipid bilayers and not in detergents? The intracellular residues 290 and 296 are located on the interface between the transport and trimerization domains in the outward-facing state, where they are well positioned to participate in the interdomain interactions. In contrast, they are distant from the interface in the inward-facing state. The opposite is true for residue 364, which is adjacent to the trimerization-domain Lys55 in the inward-facing state but not outward-facing state. Hence, we hypothesize that the nitroxide side chains, which have both hydrophobic character and hydrogen-bond acceptor potential, are engaged in the interdomain interactions and that the favorable energetic contributions of such interactions are larger in the context of the lipid bilayer compared to detergent micelles. For residue 364, we observed stabilization of the inward-facing state in membranes only in complex with aspartate but not TBOA. Consistently, in the crystal structure of the TBOA-bound Glt_{Ph}, HP2 is in an open conformation, and residue 364 is distant from the domain interface.

Quantitative analysis of the distance distributions

Because the broad experimental distributions suggested that both outward-facing and inward-facing states were present, we aimed to determine their populations. Computational predictions based on R1 rotamer libraries yielded average distances that agreed well with the experiment (**Supplementary Table 1**), but the predicted and experimental distance distributions differed substantially. Hence for quantitative analysis, we modeled the experimental data as sums of three Gaussian functions, representing the distance distributions

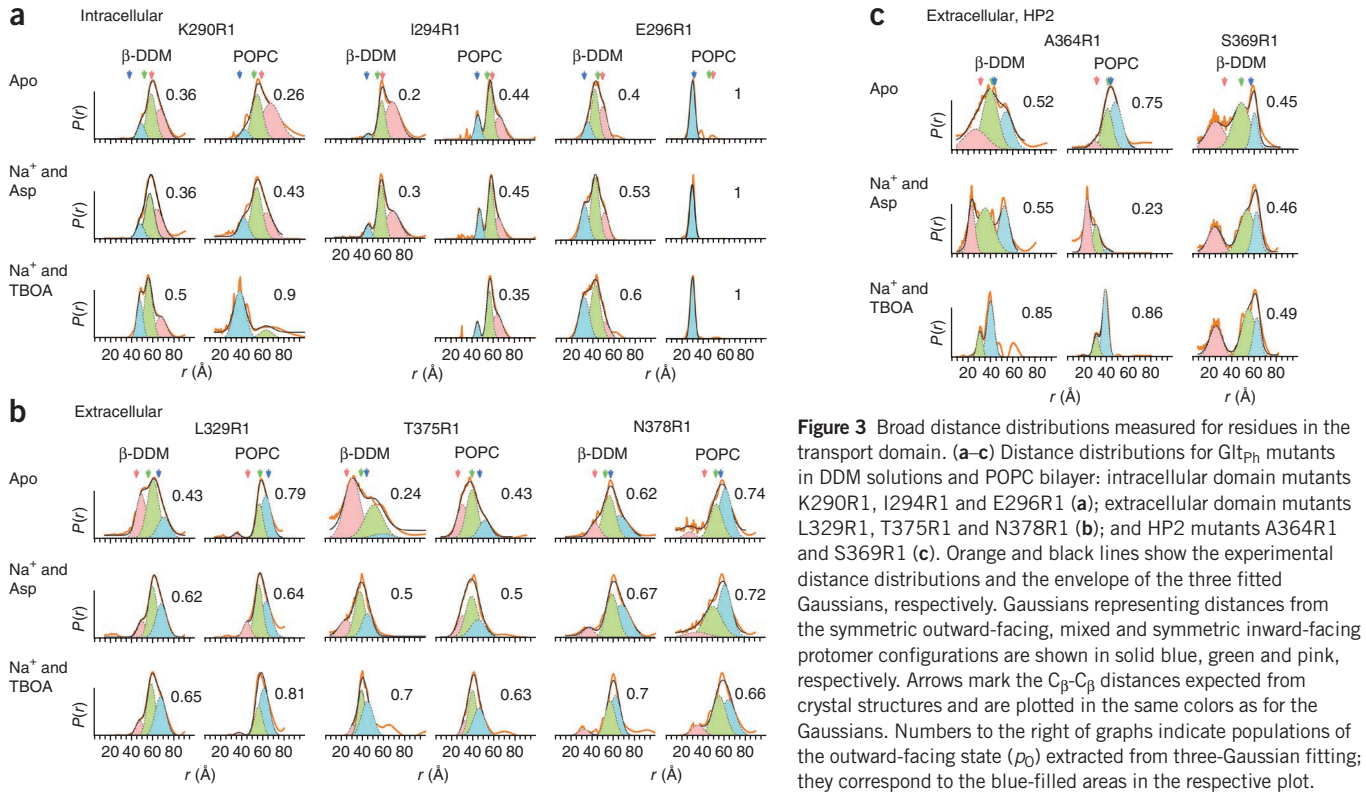

Figure 3 Broad distance distributions measured for residues in the transport domain. (**a**–**c**) Distance distributions for Glt_{Ph} mutants in DDM solutions and POPC bilayer: intracellular domain mutants K290R1, I294R1 and E296R1 (**a**); extracellular domain mutants L329R1, T375R1 and N378R1 (**b**); and HP2 mutants A364R1 and S369R1 (**c**). Orange and black lines show the experimental distance distributions and the envelope of the three fitted Gaussians, respectively. Gaussians representing distances from the symmetric outward-facing, mixed and symmetric inward-facing protomer configurations are shown in solid blue, green and pink, respectively. Arrows mark the C_β-C_β distances expected from crystal structures and are plotted in the same colors as for the Gaussians. Numbers to the right of graphs indicate populations of the outward-facing state (p_O) extracted from three-Gaussian fitting; they correspond to the blue-filled areas in the respective plot.

originating from possible configurations of the subunit pairs: both outward, both inward or mixed, that is, one outward and one inward. Assuming that the protomers isomerize between outward-facing and inward-facing states independently of each other, and taking the probability of a protomer to be in the outward-facing state as p_O, the probabilities of the two neighboring subunits facing outward or inward are p_O^2 and $(1-p_O)^2$, respectively, and the probability that they are in the mixed configurations is $2p_O(1-p_O)$. In mixed configurations, the distances from outward-facing to inward-facing and from inward-facing to outward-facing protomers are not quite the same, as the transport domain movements combine translation and rotation. Nevertheless, we represented them as a single Gaussian because increasing the number of the optimized parameters was statistically unjustified. The distance probability, $P(r)$, is then:

$$P(r) = S \times \left(\frac{p_O^2}{\sigma_O} G_O + \frac{2p_O(1-p_O)}{\sigma_M} G_M + \frac{(1-p_O)^2}{\sigma_I} G_I \right)$$

where G_O, G_M, G_I and σ_O, σ_M and σ_I are the Gaussian means (G) and s.d. (σ) for the outward-facing, mixed and inward configurations, respectively; and S is a normalization factor. The areas of the Gaussians are proportional to configuration probabilities. As initial guesses for the Gaussian means, we used either C_β-C_β distances or distances derived from modeling, which we then optimized locally in the parameter space. During the fitting process, we generally constrained the Gaussian widths to less than 6 Å, an approximate upper limit for the distance distributions measured for structured residues[30–32]. The majority of the Gaussians satisfied this criterion, with a few exceptions when broader widths had to be used to adequately represent the distributions (**Supplementary Table 1**). The resulting fits described well both the distance distributions (**Fig. 3**) and the time-domain raw data (**Supplementary Fig. 5a**). To verify the robustness of the data analysis and fitting, we varied the baseline, subtracted from the time-domain data, which gave negligible variations (**Supplementary Fig. 6b**, **Supplementary Table 2** and **Supplementary Note**).

Distances are consistent with the crystal structures

From the Gaussian fits, we extracted 139 distances, which were overall in excellent agreement with the C_β-C_β distances and with distances calculated from the rotamer libraries (**Fig. 4a** and **Supplementary Table 1**), yielding r.m.s. deviation of ~6 Å. Notably, 20 distance measurements between residues in T4 lysozyme[31] yield r.m.s. deviation of 6.9 Å, suggesting that these values reflect the inherent differences between the C_β-C_β distances and those between the paramagnetic atoms of R1. The r.m.s. deviations calculated for the subsets of distances attributed to the symmetric outward-facing and inward-facing configurations were 5.5 Å and 6.8 Å, respectively, showing that DEER data were similarly consistent with the structures of the outward-facing and inward-facing conformations (**Fig. 4b**). We also obtained similar r.m.s. deviations for measurements conducted in lipids and in detergent. However on average, distances in lipid bilayers were shorter than in detergent, suggesting that the overall protein structure was more compact (**Fig. 4c**). Finally, r.m.s. deviations for the apo, aspartate-bound and TBOA-bound Glt_{Ph} mutants in detergent were 6.2 Å, 5.9 Å and 5.9 Å, respectively, and in lipid, 5.6 Å, 4.7 Å and 6.3 Å, respectively (**Fig. 4d**), suggesting that no structural rearrangements involving the labeled residues took place that would be incompatible with the crystal structures.

The Gaussian means for the symmetric outward-facing and inward-facing configurations are scattered about the crystallographic C_β-C_β distances with a small bias toward longer distances (**Fig. 4a–d**). Such bias is typically observed for globular proteins, in which the R1 side chains are more likely to point away from the protein and from each other[37]. We also detected several outliers, for which the predicted and measured distances differed by as much as 8–15 Å (**Supplementary Table 1**). In three cases (residues 294, 364 and 378 in the inward-facing

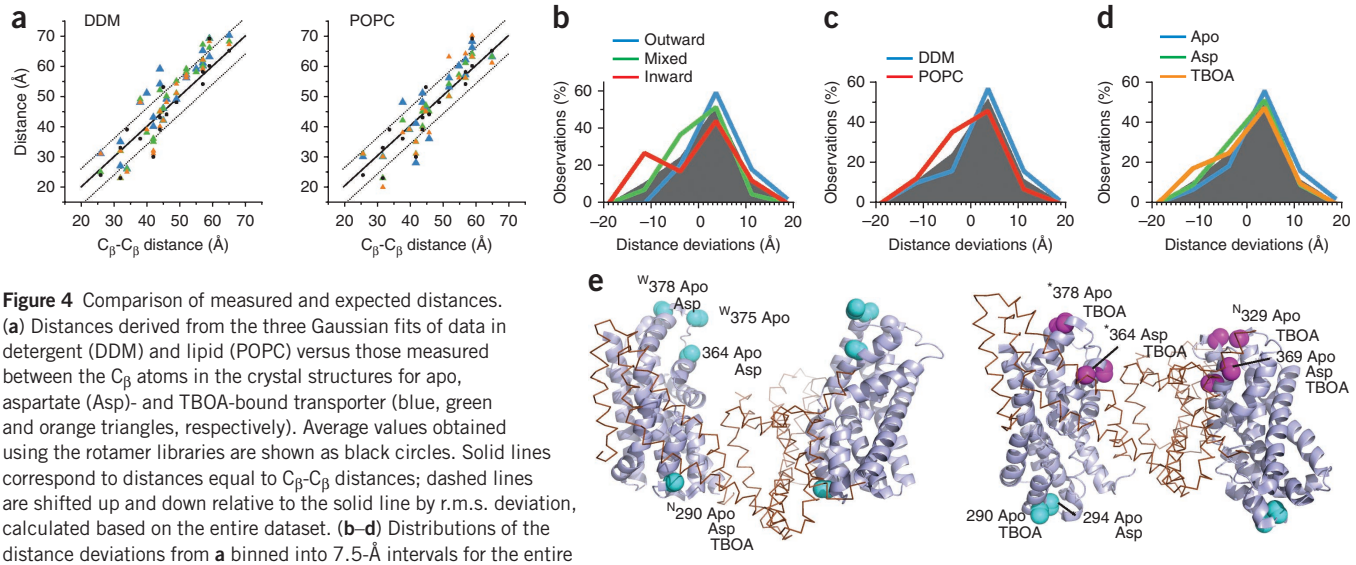

Figure 4 Comparison of measured and expected distances. (**a**) Distances derived from the three Gaussian fits of data in detergent (DDM) and lipid (POPC) versus those measured between the C_β atoms in the crystal structures for apo, aspartate (Asp)- and TBOA-bound transporter (blue, green and orange triangles, respectively). Average values obtained using the rotamer libraries are shown as black circles. Solid lines correspond to distances equal to C_β-C_β distances; dashed lines are shifted up and down relative to the solid line by r.m.s. deviation, calculated based on the entire dataset. (**b**–**d**) Distributions of the distance deviations from **a** binned into 7.5-Å intervals for the entire data set (black shaded area) or for data grouped by protomer configuration (**b**; symmetric outward, mixed and symmetric inward); environment (**c**; DDM and POPC); and the added ligand (**d**; apo, Asp-bound and TBOA-bound). (**e**) Residues showing distance deviations of at least 8 Å mapped onto the structure of Glt_{Ph} protomer pairs in outward (top) and inward (bottom) configurations. The trimerization and transport domains are shown in ribbon (brown) and cartoon representations (light blue), respectively. C_α and C_β atoms of the residues with shorter and longer distances are shown as spheres and colored magenta and cyan, respectively. The labels show the residue number and the ligand conditions under which the deviations were observed. The superscripts indicate those deviations which were in good agreement with the rotamer library predictions (*), or were associated with very wide (W) and narrow (N) distance distributions.

state), the distances predicted from the rotamer libraries were in much better agreement with the experimental distances, possibly reflecting an underlying selection of specific rotamers. In other cases, modeling did not explain the deviations, which may still be due to the selection of specific rotamers, reflect local structural flexibility or be deviations from the crystal structures. When mapped onto the protein structures, most of the outliers with longer distances were observed on the extracellular side in the outward-facing state and on the cytoplasmic side in the inward-facing state (**Fig. 4e**). In contrast, outliers with shorter distances all were on the extracellular side of the inward-facing transporter. In the latter case, the residues were part of a sterically crowded environment, possibly selecting for the R1 rotamers that point to each other. Notably, it has been shown for a mammalian homolog that the transport domains approach each other to within disulfide bond distances[38], perhaps reflecting a greater mobility range than suggested by the crystal structures. For the longer than expected distances, we note that several corresponding distance distributions are very broad and hence are more consistent with the local flexibility of the protein backbone (**Fig. 4e** and **Supplementary Table 1**).

The states have close energies

Fitted values of the outward-facing state probabilities varied between mutants. However, on average, they were 0.4–0.8 for all ligand conditions and hydrophobic environments (**Fig. 5a**), suggesting that the outward-facing and inward-facing states were similarly populated and hence, were similar in energy. We found that three Gaussian functions with areas weighted by the binomial coefficients described the data well, consistent with the individual protomers in the Glt_{Ph} trimer sampling conformational states independently of each other. Although our measurements cannot exclude subtle coupling between the subunits, we note that all-or-none transitions, such that the subunits are either all outward-facing or inward-facing, are neither required nor prohibited. Instead, we observed a range of distributions. In some, the symmetrical states were dominant, but in others the mixed states were substantially populated. These results are in agreement with the previous functional experiments, postulating independence of the subunits in Glt_{Ph} and the mammalian glutamate transporters[14,39–41]. On average, aspartate, and more so TBOA binding, modestly shifted the distributions toward the outward-facing state. These results are consistent with our recent measurements showing that the outward-facing and inward-facing states have similar affinities for Asp, and that the former binds TBOA tighter (N. Reyes, S. Oh and O.B.; unpublished data).

The wide range of p_O values obtained for various mutants may in part originate from the uncertainties of the fitting process. However, at least some of the differences can be understood from the structures, such as for the mutants on the domain interface in the lipid-reconstituted transporters discussed above. Others, such as a lower than average population of the outward-facing state in Glt_{Ph}-T375R1 in detergent cannot be easily rationalized. Nevertheless, we note that a state population change from 10% to 90% corresponds to an energy difference of only 2.6 kcal mol^{-1}, a perturbation in the expectation for single-residue mutations. Notably, all mutants exhibited some aspartate uptake (**Supplementary Fig. 6**), suggesting

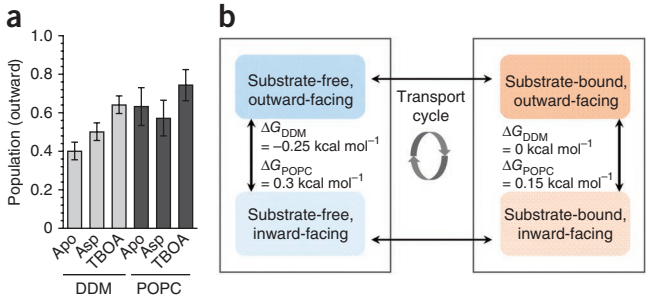

Figure 5 The inward and outward-facing states of Glt_{Ph} have close energies. (**a**) Average populations of the outward-facing state for the indicated ligand conditions (error bars, s.e.m.; $n = 8$), obtained from the Gaussian fits of data collected in detergent (DDM) and in lipid (POPC). (**b**) Transport cycle chart with the estimated free energies of the transitions from the outward-facing to inward-facing conformations.

that shifting the energy balance between the outward-facing and inward-facing states did not abrogate transport.

DISCUSSION

In membrane transporters, transitions between the outward-facing and inward-facing states are the linchpin of the catalytic mechanism. These isomerizations occur both in the substrate-loaded and substrate-free transporters to complete the cycle (**Fig. 5b**). Crystal structures of the wild-type Glt_{Ph} have pictured the protein in symmetric outward-facing states[6,7]. The structure of the symmetric inward-facing state had been determined by trapping the transporter using mercury-mediated crosslinking of two cysteines placed on the domain interface[8] and later recapitulated in the absence of the crosslinks[9]. These structures pictured the outward-to-inward transition involving a large-scale transmembrane movement of the transport domain. Here we demonstrated that these domain motions occur in detergent solution and, importantly, in membranes. We also developed a more complete picture of the conformational ensemble of the transporter by showing that the outward-facing and inward-facing states had similar energies both when the transporter was fully loaded with Na^+ and aspartate and empty. Our measurements were consistent with the lack of either positive or negative cooperativity between the subunits of the trimer, picturing Glt_{Ph} as a system of three largely independent protomers sampling the outward-facing and inward-facing states. Glt_{Ph} originates from a hyper-thermophilic archaeon and normally functions at 100 °C, where it is expected to better match the kinetic properties of the mammalian glutamate transporters[10]. At present, we do not know what the state distributions are at these temperatures. Extrapolations based on the binding experiments suggest that Na^+ and aspartate affinity for the outward-facing state of Glt_{Ph} is higher than that for the inward-facing state at elevated temperatures (N. Reyes, S. Oh and O.B.; unpublished data), a property also reported for the mammalian homologs at physiological temperature[42]. Hence, in these systems the ligands will stabilize the outward-facing conformation more substantially than we observed here.

The mechanisms by which lipid bilayers stabilize specific conformations of membrane proteins, thereby modulating their function, have been extensively scrutinized with particular emphasis on the role of the hydrophobic mismatch between the proteins and the bilayer, and on specific interactions with lipids[43–45]. In Glt_{Ph}, the structural studies suggest that the movements of the transport domain would result in remodeling of the transport domain interface with the surrounding membrane. Hence, it is unexpected that transferring Glt_{Ph} from the dynamic detergent micelles into the relatively rigid lipid bilayers has only a modest effect on the conformational ensemble. We observed an increase of the outward-facing state population of only ~10–20% on average, corresponding to ~0.5 kcal mol^{-1} more favorable free energy in lipid compared to detergent (**Fig. 5**). However, the effects of the lipid environment were more pronounced in several mutants, including E296R1, A364R1 and K290R1, where we observed single dominant conformations in lipids. The observed population shifts cannot be attributed to R1 side chains interacting with the lipid or detergent directly. Instead, they can be rationalized in terms of R1 interactions on the interface between the transport and trimerization domains, which become more favorable in membranes. This opens an interesting possibility that intra- and interprotomer bond formation in membrane proteins may be more favorable in lipid bilayers than in more disordered detergent micelles. Consistently, a greater contribution of the interprotomer hydrogen bond to the stability of glycophorin A dimer in native membranes compared to detergent has been reported[46]. We also observed that average distances in lipid were shorter than in detergent, suggesting that the overall protein structure is more compact, perhaps leading to greater constraints on the interfacial protein side chains, smaller loss of the conformational entropy upon bond formation and hence more favorable free energies. Such effects may contribute to the repertoire of mechanisms by which the bilayer alters the energetics of membrane proteins.

Whether the closely matching energies of the outward-facing and inward-facing states is a general phenomenon in transporters remains to be elucidated. In lactose permease LacY, the cysteine accessibility studies suggest that the apo transporter is predominantly inward-facing and that sugar binding favors the outward-facing states[47]. However, similarly to our results, DEER data on LacY showed that multiple conformations were populated under all ligand conditions[48]. Also, sodium and hydantoin symporter Mhp1 crystallized in both outward-facing and inward-facing conformations under similar conditions[49,50], suggesting that the two states were close in energy and well populated. Finally, theoretical considerations suggest that balancing the relative energies of the states would maximize the turnover rates[44]. Here we describe a robust method to probe state distributions of transporters under native-like conditions of the lipid bilayers, which can be applied to a wide range of systems. Our approach opens a way to investigate whether and how the nature of the lipid environment affects the conformational selection and to establish a correspondence between the relative energies of the outward-facing and inward-facing states, and substrate transport rates. It would be important to investigate whether the thickness of the lipid bilayer, its fluidity or specific lipid composition affect the state distributions as well as to probe whether these membrane properties alter the strength of specific interdomain interactions.

METHODS

Methods and any associated references are available in the online version of the paper.

Note: Supplementary information is available in the online version of the paper.

ACKNOWLEDGMENTS

The work was supported by US National Institute of Neurological Disorders and Stroke grants NS064357 and NS064357-02S1 and a grant from Bohmfalk Charitable Trust to O.B., and US National Center for Research Recourses grant P41-RR016292, US National Institute of General Medical Sciences grant P41GM103521 and US National Institute of Biomedical Imaging and Bioengineering grant R010EB003150 J.H.F.

AUTHOR CONTRIBUTIONS

E.R.G. and O.B. developed the mutation strategy for DEER spectroscopy, and designed the molecular biology and biochemical part of the experiments. E.R.G., P.P.B. and J.H.F. designed the DEER spectroscopy experiments. E.R.G. performed most of the DEER spectroscopy experiments, protein expression and purification, and spin labeling. C.G. carried out the mutagenesis and participated in protein expression and purification. P.P.B. performed some of the DEER measurements. E.R.G., O.B. and P.P.B. analyzed the data. O.B., E.R.G., P.P.B. and J.H.F. wrote the manuscript.

COMPETING FINANCIAL INTERESTS

The authors declare no competing financial interests.

Published online at http://www.nature.com/doifinder/10.1038/nsmb.2494.
Reprints and permissions information is available online at http://www.nature.com/reprints/index.html.

1. Danbolt, N.C. Glutamate uptake. *Prog. Neurobiol.* **65**, 1–105 (2001).
2. Hinoi, E., Takarada, T., Tsuchihashi, Y. & Yoneda, Y. Glutamate transporters as drug targets. *Curr. Drug Targets CNS Neurol. Disord.* **4**, 211–220 (2005).
3. Levy, L.M., Warr, O. & Attwell, D. Stoichiometry of the glial glutamate transporter GLT-1 expressed inducibly in a Chinese hamster ovary cell line selected for low endogenous Na+-dependent glutamate uptake. *J. Neurosci.* **18**, 9620–9628 (1998).

4. Zerangue, N. & Kavanaugh, M.P. Flux coupling in a neuronal glutamate transporter. *Nature* **383**, 634–637 (1996).
5. Owe, S.G., Marcaggi, P. & Attwell, D. The ionic stoichiometry of the GLAST glutamate transporter in salamander retinal glia. *J. Physiol. (Lond.)* **577**, 591–599 (2006).
6. Yernool, D., Boudker, O., Jin, Y. & Gouaux, E. Structure of a glutamate transporter homologue from *Pyrococcus horikoshii*. *Nature* **431**, 811–818 (2004).
7. Boudker, O., Ryan, R.M., Yernool, D., Shimamoto, K. & Gouaux, E. Coupling substrate and ion binding to extracellular gate of a sodium-dependent aspartate transporter. *Nature* **445**, 387–393 (2007).
8. Reyes, N., Ginter, C. & Boudker, O. Transport mechanism of a bacterial homologue of glutamate transporters. *Nature* **462**, 880–885 (2009).
9. Verdon, G. & Boudker, O. Crystal structure of an asymmetric trimer of a bacterial glutamate transporter homolog. *Nat. Struct. Mol. Biol.* **19**, 355–357 (2012).
10. Ryan, R.M., Compton, E.L. & Mindell, J.A. Functional characterization of a Na^+-dependent aspartate transporter from *Pyrococcus horikoshii*. *J. Biol. Chem.* **284**, 17540–17548 (2009).
11. Groeneveld, M. & Slotboom, D.J. Na^+: aspartate coupling stoichiometry in the glutamate transporter homologue GltPh. *Biochemistry* **49**, 3511–3513 (2010).
12. Yernool, D., Boudker, O., Folta-Stogniew, E. & Gouaux, E. Trimeric subunit stoichiometry of the glutamate transporters from *Bacillus caldotenax* and *Bacillus stearothermophilus*. *Biochemistry* **42**, 12981–12988 (2003).
13. Gendreau, S. *et al.* A trimeric quaternary structure is conserved in bacterial and human glutamate transporters. *J. Biol. Chem.* **279**, 39505–39512 (2004).
14. Groeneveld, M. & Slotboom, D.J. Rigidity of the subunit interfaces of the trimeric glutamate transporter GltT during translocation. *J. Mol. Biol.* **372**, 565–570 (2007).
15. Focke, P.J., Moenne-Loccoz, P. & Larsson, H.P. Opposite movement of the external gate of a glutamate transporter homolog upon binding cotransported sodium compared with substrate. *J. Neurosci.* **31**, 6255–6262 (2011).
16. Huang, Z. & Tajkhorshid, E. Dynamics of the extracellular gate and ion-substrate coupling in the glutamate transporter. *Biophys. J.* **95**, 2292–2300 (2008).
17. Shrivastava, I.H., Jiang, J., Amara, S.G. & Bahar, I. Time-resolved mechanism of extracellular gate opening and substrate binding in a glutamate transporter. *J. Biol. Chem.* **283**, 28680–28690 (2008).
18. Borbat, P.P. & Freed, J.H. Measuring distances by pulsed dipolar ESR spectroscopy: spin-labeled histidine kinases. *Methods Enzymol.* **423**, 52–116 (2007).
19. Borbat, P.P. & Freed, J.H. Pros and cons of pulse dipolar ESR: DQC and DEER. *EPR Newsletter* **17**, 21–33 (2007).
20. Mchaourab, H.S., Steed, P.R. & Kazmier, K. Toward the fourth dimension of membrane protein structure: insight into dynamics from spin-labeling EPR spectroscopy. *Structure* **19**, 1549–1561 (2011).
21. Reginsson, G.W. & Schiemann, O. Pulsed electron-electron double resonance: beyond nanometre distance measurements on biomacromolecules. *Biochem. J.* **434**, 353–363 (2011).
22. Borbat, P.P. *et al.* Conformational motion of the ABC transporter MsbA induced by ATP hydrolysis. *PLoS Biol.* **5**, e271 (2007).
23. Tong, J., Borbat, P.P., Freed, J.H. & Shin, Y.K. A scissors mechanism for stimulation of SNARE-mediated lipid mixing by cholesterol. *Proc. Natl. Acad. Sci. USA* **106**, 5141–5146 (2009).
24. Georgieva, E.R., Ramlall, T.F., Borbat, P.P., Freed, J.H. & Eliezer, D. Membrane-bound alpha-synuclein forms an extended helix: long-distance pulsed ESR measurements using vesicles, bicelles, and rodlike micelles. *J. Am. Chem. Soc.* **130**, 12856–12857 (2008).
25. Georgieva, E.R., Ramlall, T.F., Borbat, P.P., Freed, J.H. & Eliezer, D. The lipid-binding domain of wild type and mutant alpha-synuclein: compactness and interconversion between the broken and extended helix forms. *J. Biol. Chem.* **285**, 28261–28274 (2010).
26. Upadhyay, A.K., Borbat, P.P., Wang, J., Freed, J.H. & Edmondson, D.E. Determination of the oligomeric states of human and rat monoamine oxidases in the outer mitochondrial membrane and octyl beta-D-glucopyranoside micelles using pulsed dipolar electron spin resonance spectroscopy. *Biochemistry* **47**, 1554–1566 (2008).
27. Vamvouka, M., Cieslak, J., Van Eps, N., Hubbell, W. & Gross, A. The structure of the lipid-embedded potassium channel voltage sensor determined by double-electron-electron resonance spectroscopy. *Protein Sci.* **17**, 506–517 (2008).
28. Claxton, D.P. *et al.* Ion/substrate-dependent conformational dynamics of a bacterial homolog of neurotransmitter:sodium symporters. *Nat. Struct. Mol. Biol.* **17**, 822–829 (2010).
29. Joseph, B., Jeschke, G., Goetz, B.A., Locher, K.P. & Bordignon, E. Transmembrane gate movements in the type II ATP-binding cassette (ABC) importer BtuCD-F during nucleotide cycle. *J. Biol. Chem.* **286**, 41008–41017 (2011).
30. Borbat, P.P., Mchaourab, H.S. & Freed, J.H. Protein structure determination using long-distance constraints from double-quantum coherence ESR: study of T4 lysozyme. *J. Am. Chem. Soc.* **124**, 5304–5314 (2002).
31. Kazmier, K., Alexander, N.S., Meiler, J. & Mchaourab, H.S. Algorithm for selection of optimized EPR distance restraints for *de novo* protein structure determination. *J. Struct. Biol.* **173**, 549–557 (2011).
32. Georgieva, E.R. *et al.* Effect of freezing conditions on distances and their distributions derived from double electron electron resonance (DEER): a study of doubly-spin-labeled T4 lysozyme. *J. Magn. Reson.* **216**, 69–77 (2012).
33. Polyhach, Y., Bordignon, E. & Jeschke, G. Rotamer libraries of spin labelled cysteines for protein studies. *Phys. Chem. Chem. Phys.* **13**, 2356–2366 (2011).
34. Bhatnagar, J. *et al.* Structure of the ternary complex formed by a chemotaxis receptor signaling domain, the CheA histidine kinase, and the coupling protein CheW as determined by pulsed dipolar ESR spectroscopy. *Biochemistry* **49**, 3824–3841 (2010).
35. Jeschke, G., Sajid, M., Schulte, M. & Godt, A. Three-spin correlations in double electron-electron resonance. *Phys. Chem. Chem. Phys.* **11**, 6580–6591 (2009).
36. Shimamoto, K. *et al.* DL-threo-beta-benzyloxyaspartate, a potent blocker of excitatory amino acid transporters. *Mol. Pharmacol.* **53**, 195–201 (1998).
37. Bhatnagar, J., Freed, J.H. & Crane, B.R. Rigid body refinement of protein complexes with long-range distance restraints from pulsed dipolar ESR. *Methods Enzymol.* **423**, 117–133 (2007).
38. Jiang, J., Shrivastava, I.H., Watts, S.D., Bahar, I. & Amara, S.G. Large collective motions regulate the functional properties of glutamate transporter trimers. *Proc. Natl. Acad. Sci. USA* **108**, 15141–15146 (2011).
39. Grewer, C. *et al.* Individual subunits of the glutamate transporter EAAC1 homotrimer function independently of each other. *Biochemistry* **44**, 11913–11923 (2005).
40. Koch, H.P. & Larsson, H.P. Small-scale molecular motions accomplish glutamate uptake in human glutamate transporters. *J. Neurosci.* **25**, 1730–1736 (2005).
41. Leary, G.P., Stone, E.F., Holley, D.C. & Kavanaugh, M.P. The glutamate and chloride permeation pathways are colocalized in individual neuronal glutamate transporter subunits. *J. Neurosci.* **27**, 2938–2942 (2007).
42. Zhang, Z. *et al.* Transport direction determines the kinetics of substrate transport by the glutamate transporter EAAC1. *Proc. Natl. Acad. Sci. USA* **104**, 18025–18030 (2007).
43. Phillips, R., Ursell, T., Wiggins, P. & Sens, P. Emerging roles for lipids in shaping membrane-protein function. *Nature* **459**, 379–385 (2009).
44. Andersen, O.S. & Koeppe, R.E., II. Bilayer thickness and membrane protein function: an energetic perspective. *Annu. Rev. Biophys. Biomol. Struct.* **36**, 107–130 (2007).
45. Lee, A.G. How lipids affect the activities of integral membrane proteins. *Biochim. Biophys. Acta* **1666**, 62–87 (2004).
46. Duong, M.T., Jaszewski, T.M., Fleming, K.G. & MacKenzie, K.R. Changes in apparent free energy of helix-helix dimerization in a biological membrane due to point mutations. *J. Mol. Biol.* **371**, 422–434 (2007).
47. Kaback, H.R. *et al.* Site-directed alkylation and the alternating access model for LacY. *Proc. Natl. Acad. Sci. USA* **104**, 491–494 (2007).
48. Smirnova, I. *et al.* Sugar binding induces an outward facing conformation of LacY. *Proc. Natl. Acad. Sci. USA* **104**, 16504–16509 (2007).
49. Weyand, S. *et al.* Structure and molecular mechanism of a nucleobase-cation-symport-1 family transporter. *Science* **322**, 709–713 (2008).
50. Shimamura, T. *et al.* Molecular basis of alternating access membrane transport by the sodium-hydantoin transporter Mhp1. *Science* **328**, 470–473 (2010).

ONLINE METHODS

Molecular biology and protein purification. Mutations encoding cysteine substitutions were introduced in the sequence encoding cysteine-less seven-histidine Glt_{Ph} variant[8] using standard techniques and verified by DNA sequencing. All mutants were expressed and purified as described previously[6]. Briefly, C-terminal $(His)_8$ fusion constructs were expressed in *Escherichia coli* DH10B cells (Invitrogen) and purified by metal affinity chromatography. The tag was removed by thrombin digestion, and the proteins were further purified by size-exclusion chromatography. The final protein concentration of trimers was 15–30 μM, calculated from absorbance at 280 nm using coefficient of 26, 820 M^{-1} cm^{-1} (per monomer). Samples were stored at –80 °C and further manipulated in buffer A containing in 20 mM HEPES, pH 7.4, 100 mM NaCl, 0.1 mM aspartate and 1 mM DDM.

Spin-labeling and preparation of samples for DEER spectroscopy. All mutants were spin-labeled with S-(2,2,5,5-tetramethyl-2,5-dihydro-1H-pyrrol-3-yl)methyl methanesulfonothioate (MTSL; Toronto Research Chemicals) in buffer A. MTSL was first dissolved in acetonitrile and added to the protein solutions in 20–30-fold (per monomer) molar excess. The labeling was performed for 3 h at room temperature and continued overnight at 4 °C with agitation. The unreacted label was removed by dialysis against four changes of 30 ml of buffer A over 30 h using 25-kDa molecular weight cutoff membrane. To prepare substrate-free Glt_{Ph}, buffer B, containing 20 mM HEPES, pH 7.4, 100 mM KCl and 1 mM DDM, was used during the last two buffer changes. When apo protein samples were prepared for reconstitution into the bilayers, buffer B was supplemented with 2.5 mM NaCl. TBOA-bound protein was prepared starting with apo protein by adding NaCl and TBOA (Tocris Bioscience) to 50 mM and 125 μM, respectively. Glt_{Ph} mutants were reconstituted into POPC (Avanti Polar Lipids) membranes at protein to lipid molar ratio of 1:2,400 in DDM-free buffer A or buffer B, containing 2.5 mM NaCl. Aliquots of chloroform-solubilized POPC were dried under vacuum and rehydrated at 50 mM using appropriate buffers. The lipid bilayers were destabilized by the addition of Triton X-100 to the final lipid:Triton X-100 ratio of 1:0.6 (w/w), and incubated with protein for 1 h at room temperature. Prewashed Bio-Beads (Bio-Rad) were equilibrated in the appropriate buffer, added to the mixtures of protein and lipid at 100 mg/ml, and incubated at room temperature for 2 h. The liposome suspension was filtered, supplemented with fresh beads and incubated for 4 h at 4 °C. The procedure was repeated twice. The multilayer vesicles were collected by centrifugation at 70,000*g* for 15 min. The vesicles containing apo Glt_{Ph} were additionally washed three times by loading with DDM-free buffer B using freeze and thaw procedure followed by centrifugation. To prepare TBOA-bound lipid-reconstituted samples, the vesicles were washed in the same manner in buffer supplemented with NaCl and TBOA at 50 mM and 125 μM, respectively. The final concentration of the spin-labeled Glt_{Ph} trimer in both DDM and POPC samples was 10–55 μM, based on the standard calibrated measurement of the primary echo amplitude, which gave total spin concentration. The reference sample was 200 μM 4-hydroxy-2,2,6,6-tetramethylpiperidin-1-oxyl (TEMPOL) in 50% (w/v) glycerol-d8/D_2O[25]. The final Glt_{Ph} trimer to lipid molar ratio was 1:2,400, and lipid concentration was ~75 mg/ml. All samples were prepared in the final buffer containing 90% D_2O with protein samples in DDM also supplemented with glycerol-d8 at 20% (w/v). Samples were loaded into 1.8 inner diameter custom Pyrex sample tubes (Wilmad-LabGlass), and shock-frozen in liquid N_2 before DEER measurements. Samples were prepared and measured at least twice.

DEER measurements. Measurements were performed at 60 K as previously described[32] using a 17.3 GHz home-built Ku-band pulse spectrometer[51], which has provided high-sensitivity measurements in previous studies[18,19,22–26,32,34,52]. A standard four-pulse DEER sequence[53] with π/2-π-π pulse widths of 16 ns, 32 ns and 32 ns, respectively, and a 32 ns π pump pulse was used routinely. When testing the three-spin effects, a 14-ns pump pulse with varied flip angles was used (**Supplementary Note**). The frequency separation between detection and pump pulses was 70 MHz. The detection pulses were positioned at the low-field edge of the nitroxide spectrum. Typical dipolar evolutions times were 1.5–5 μs as needed with signal averaging from 2 h to 20 h. The homogeneous background was removed from the raw time-domain signals and the distances were reconstructed from the baseline-corrected and normalized signals by using Tikhonov regularization method[54] and refined by maximum entropy method (**Supplementary Note**)[55].

Modeling of distance distributions and data analysis. To model expected distance distributions, we used rotamer libraries generated by molecular modeling software MMM[33]. The ensembles of statistically weighed spin-label conformers were calculated at 175 K. The crystal structures of Glt_{Ph} in the outward-facing conformation with substrate (PDB: 2NWX) or TBOA (PDB: 2NWW) and inward-facing conformation with substrate (PDB: 3KBC) were used as templates for the calculations. In addition, we generated a structural model containing two protomers in the outward-facing and one protomer in the inward-facing conformation. The model construction was straightforward because the conformations of the trimerization domains are similar in the outward-facing and inward-facing states, and there are no steric clashes. For the mixed states, we calculated the average distance distributions from outward-facing to inward-facing and from inward-facing to outward-facing protomers. The experimental distance distributions were fitted to a single Gaussian for residues in the trimerization domain and to a scaled sum of three Gaussians for residues in the transport domain using nonlinear curve fitting algorithm in OriginLab software (OriginLab). As initial guesses for the Gaussians means, we used the average distances calculated by MMM, or the C_β-C_β distances in the crystal structures and the structural model.

Activity assay. For the transport activity measurements, spin-labeled and unlabeled Glt_{Ph} mutants were reconstituted in POPC liposomes at protein to lipid ratio of 1:100 as previously described[7,10]. Porteoliposomes were loaded with buffer containing in 20 mM HEPES, pH 7.4, 100 mM KCl and 200 mM choline chloride, extruded through 0.4 μm nitrocellulose filters and incubated for 2 min at 30 °C in buffer containing 20 mM HEPES, pH 7.4, 100 mM KCl, 200 mM NaCl and 600 nM [^{3}H]L-aspartate. The uptake reactions were terminated by diluting proteoliposomes into ice-cold buffer, vesicles were collected by filtration, and retained radioactivity was measured[7,10].

51. Borbat, P.P., Crepeau, R.H. & Freed, J.H. Multifrequency two-dimensional Fourier transform ESR: an X/Ku-band spectrometer. *J. Magn. Reson.* **127**, 155–167 (1997).
52. Borbat, P.P. & Freed, J.H. Pulse dipolar ESR: distance measurements. in *Structural Information from Spin-Labels and Intrinsic Paramagnetic Centres in the Biosciences. Structure and Bonding.* (eds., Harmer, J. & Timmel, C.) (Springer, Berlin, 2012).
53. Pannier, M., Veit, S., Godt, A., Jeschke, G. & Spiess, H.W. Dead-time free measurement of dipole-dipole interactions between electron spins. *J. Magn. Reson.* **142**, 331–340 (2000).
54. Chiang, Y.W., Borbat, P.P. & Freed, J.H. The determination of pair distance distributions by pulsed ESR using Tikhonov regularization. *J. Magn. Reson.* **172**, 279–295 (2005).
55. Chiang, Y.W., Borbat, P.P. & Freed, J.H. Maximum entropy: a complement to Tikhonov regularization for determination of pair distance distributions by pulsed ESR. *J. Magn. Reson.* **177**, 184–196 (2005).

doi:10.1038/nsmb.2494